Tolerance allocation Based on the Minimum Deformation Zone of Finite Element Structural Frame Analysis

Ahmad Barari[1]

[1]University of Ontario Institute of Technology, Ahmad.Barari@uoit.ca

ABSTRACT

As a design and manufacturing principle the combination of the actual deformations in a designed mechanical part due to all of its service loads and the deviations due to all of its manufacturing and production uncertainties should be equal or less than its maximum acceptable total geometric and topological deviations that can satisfy its form, fit, and function requirements. Therefore, precise knowledge of the actual deformations of mechanical components under the applied loads and boundary conditions need to be used to allocate suitable tolerances. However, this process is optimized only if the minimum geometric zone that covers the evaluated deformations is studied properly. In order to achieve this goal, the concept of minimum deformation zone is introduced in this paper. Using this concept, a unified methodology is developed to find the optimum tolerances for the geometric parameters of mechanical frame structures. Validity of the developed procedure is studied by conducting case studies and variety of experiments. The developed methodology can be employed efficiently during detailed design process in a Computer Aided Design environment.

Keywords: tolerance analysis, minimum deformation zone, geometric deviations.
DOI: 10.3722/cadaps.2013.629-641

1 INTRODUCTION

Transfer of accuracy though the different stages of design and manufacturing is a major concern in the Product Life-Cycle Management (PLM). The required geometric and dimensional accuracies of various features in the final product are analysed and decided during the design stage. These design specifications are documented in the form of Geometric Dimensioning and Tolerancing (GD&T) standards to be issued to the other PLM activities. Allocation of these tolerances should be conducted based on precise understanding of actual elastic/plastic deformations of parts and components under to all service loads and also the geometric and dimensional deviations due to all the inherent error

sources in manufacturing and assembly processes. Therefore, the total acceptable range of geometric and topologic deviations from the ideal design that still can satisfy functionality, form, and fitting requirements of the product need to be able to cover the range of manufacturing and production errors as well as the expected deformations due to working loads and condition. This relationship can be simply expressed as:

$$\Delta G = G_F \ominus G_I \quad \text{Eqn. 1}$$

$$\Delta G = \delta_e \oplus \delta_d \quad \text{Eqn. 2}$$

where ΔG is the maximum zone calculated by operator $\ominus$ between two geometries of G_F and G_I. G_F and G_I refer to the functioning final geometry of the part during working condition, and the initial ideal geometry of the designed part, respectively. δ_d is a combination of all deformation vectors that represents deformation of the part due to applied loads, and δ_e is a combination of all deviation vectors due to manufacturing and assembly errors. Operator $\oplus$ produces addition and interaction of the two arguments. Considering the small quantities of δ_d and δ_e comparing to the geometry of the part, interactions between two sets of vectors of δ_d and δ_e can be neglected, and using superposition concept we can estimate:

$$\Delta G \cong \delta_e + \delta_d \quad \text{Eqn. 3}$$

It is highly important for designers to have a good understanding of δ_d and a valid estimation of δ_e before allocating design tolerances. Showing the set of evaluated deformation vectors due to applied loads by $\widehat{\delta_d}$ and the estimation set of production errors vectors by $\widehat{\delta_e}$, and by applying the superposition concept the allocated design tolerances, t, can be calculated as:

$$t = \alpha \widehat{\delta_e} \cong \alpha (G_F \ominus G_I - \widehat{\delta_d}) \quad \text{Eqn. 4}$$

where the final geometry of the part during working condition, G_F, and the ideal geometry of the designed part, G_I, are the specifications that are already defined by the designers, $\widehat{\delta_d}$ is the set of evaluated deformation vectors due to applied loads, and α is a set of safety factors to compensate for under/overestimations of production errors or simplifications in evaluating deformations. The safety factors required for evaluation of deformations reflect the existing uncertainties in the modeling, loading, and analyses of the structure. Proper estimation of safety factors needs accurate knowledge of simplifications applied to the model and their consequences, worst case working condition of the mechanical assembly or structure, and established assumptions in the analysis.

Using Equation 4, designers will be able to calculate tolerances for all of the geometric properties of parts. However, in a concurrent engineering platform, a good designer also needs to consider manufacturing cost and restrictions. Usually allocating tighter tolerances needs to be satisfied by more expensive, more accurate, and more time consuming manufacturing processes. Therefore, it is crucial to properly calculate terms in Equation 4 during tolerance allocation.

A method to optimize design tolerances by more accurate analyze of the terms in Equation 4 is presented. In this methodology the allocated tolerances are maximized by minimizing the zone that covers the entire ideal geometry and all the deformation vectors. This method uses a Finite Element Analysis (FEA) approach to evaluate the deformation vectors. Without losing the generality, this

tolerance allocation concept is implemented for the structure with beams and frame elements under static loading and case study of an automotive structure is used for validation of the process.

2 BACKGROUND

Many designers only use the first expression in Equation 4 for the tolerance allocation process. Tolerance allocation research similar to work reported in [1- 3] is conducted whit this approach, and analytical, experimental, or numerical approaches are employed to achieve this goal. They basically try to estimate the manufacturing and production errors, $\widehat{\delta_e}$, and allocate the tolerances, t, accordingly. However, this approach doesn't reflect and asses the final desired geometry, G_F, under the loading condition. Therefore, the approach cannot lead always to a robust design.

Alternatively, the approach presented in this work is to use the second expression in Equation 4 to achieve the most appropriate tolerance allocation. Basically, this approach allows the designers to maintain the final desired geometry of the product while concurrently they try to maximize the range of allocated tolerances. This approach will automatically make the required manufacturing processes less expensive and more practical.

In order to use this approach, both analytical or numerical solutions can be used during the design process to evaluate the deformation vectors, $\widehat{\delta_d}$. Since the analytical solutions are limited to application of primitives and simple geometries, in order to develop a unified tolerance allocation approach this research is focused to utilize general purpose numerical FEA solutions. The methodology is implemented for frame structures with beam 2 nodes elements.

The finite element solver developed for the structural models uses typical beam elements with linear shape functions and Galerkin's Method is used for deriving the beam element equations [4]. The method divides the structure into nodes and beams (elements). Nodes occur wherever elements intersect and are associated with the degrees of freedom. The nodes for the beam element each have six degrees of freedom, three in translation along each axis and three for rotation about each axis. The set of displacement vectors, $\widehat{\delta_d}$, can be found using:

$$\widehat{\delta_d} = K^{-1}F \qquad \text{Eqn. 5}$$

where matrix K is the overall assembly stiffness matrix of the entire part or the structure under loading, and F is the vector of all nodal forces and boundary conditions. In the finite element method for structural design, a stiffness matrix is a symmetric, positive, and semi- definite matrix that generalizes the stiffness of Hooke's law to a matrix, describing the stiffness of all of the degrees of freedom so that the vector of applied forces can be calculated by multiplying this matrix to the vector of displacements. The assembly stiffness matrix is an assembly of the corresponding stiffness matrices of all elements. Each individual beam element will have a corresponding stiffness matrix that relates the element forces with the nodal displacements. The beam element's stiffness matrix employed in this work for i^{th} element is as follows:

$$K_i^e = \begin{bmatrix} \frac{EA}{L} & 0 & 0 & 0 & 0 & 0 & \frac{-EA}{L} & 0 & 0 & 0 & 0 & 0 \\ 0 & \frac{12EI_z}{L^3} & 0 & 0 & 0 & \frac{6EI_z}{L^2} & 0 & \frac{-12EI_z}{L^3} & 0 & 0 & 0 & \frac{6EI_z}{L^2} \\ 0 & 0 & \frac{12EI_y}{L^3} & 0 & \frac{-6EI_y}{L^2} & 0 & 0 & 0 & \frac{-12EI_y}{L^3} & 0 & \frac{-6EI_y}{L^2} & 0 \\ 0 & 0 & 0 & \frac{GJ}{L} & 0 & 0 & 0 & 0 & 0 & \frac{-GJ}{L} & 0 & 0 \\ 0 & 0 & \frac{-6EI_y}{L^2} & 0 & \frac{4EI_y}{L} & 0 & 0 & 0 & \frac{6EI_y}{L^2} & 0 & \frac{2EI_y}{L} & 0 \\ 0 & \frac{6EI_z}{L^2} & 0 & 0 & 0 & \frac{4EI_z}{L} & 0 & \frac{-6EI_z}{L^2} & 0 & 0 & 0 & \frac{2EI_z}{L} \\ \frac{-EA}{L} & 0 & 0 & 0 & 0 & 0 & \frac{EA}{L} & 0 & 0 & 0 & 0 & 0 \\ 0 & \frac{-12EI_z}{L^3} & 0 & 0 & 0 & \frac{-6EI_z}{L^2} & 0 & \frac{12EI_z}{L^3} & 0 & 0 & 0 & \frac{-6EI_z}{L^2} \\ 0 & 0 & \frac{-12EI_y}{L^3} & 0 & \frac{6EI_y}{L^2} & 0 & 0 & 0 & \frac{12EI_y}{L^3} & 0 & \frac{12EI_z}{L^3} & 0 \\ 0 & 0 & 0 & \frac{-GJ}{L} & 0 & 0 & 0 & 0 & 0 & \frac{GJ}{L} & 0 & 0 \\ 0 & 0 & \frac{-6EI_y}{L^2} & 0 & \frac{2EI_y}{L} & 0 & 0 & 0 & \frac{12EI_z}{L^3} & 0 & \frac{4EI_y}{L} & 0 \\ 0 & \frac{6EI_z}{L^2} & 0 & 0 & 0 & \frac{2EI_z}{L} & 0 & \frac{-6EI_z}{L^2} & 0 & 0 & 0 & \frac{4EI_z}{L} \end{bmatrix} \quad \text{Eqn. 6}$$

In the above equation A is the cross-sectional area, I_y and I_z are moment of inertia corresponding to y and z directions respectively when the element is aligned with x-direction in its local coordinate system, J is the polar moment of inertia, E is Young's modulus, G is the shear modulus of elasticity, and L is the length of the i^{th} element. Considering our FEA-based approach and Equation 5, Equation 6 can be expressed as:

$$t = \alpha\,(G_F \ominus G_I - K^{-1}F) \quad \text{Eqn. 7}$$

where G_F is the final geometry of the part during working condition, G_I is the ideal geometry of the designed part, K is the overall assembly stiffness matrix of the entire part or the structure under loading, F is the vector of all nodal forces and boundary conditions, and α is a set of safety factors. Having all these terms specified, the only challenge to calculate tolerances, t, will be a proper definition of operator $\ominus$ in Equation 7. The research attempts in this area, similar to the work reported in [5], usually neglected that this operator needs to evaluate the maximum or the largest zone between the two geometries and what can be achieved by simple subtracting the two geometries is not necessarily the largest zone between them.

Since the geometric representation of the FEA output for deformations is in form of discrete displacement vectors, the operator $\ominus$ needs to find the best fit between the ideal geometry, G_I, and a group of discrete points specified by $\widehat{\delta_d}$ to maximize $G_F \ominus G_I - K^{-1}F$.

Fitting of a given geometry to a group of discrete points is a challenging research area and the computational algorithms developed for this task are subject to many sources of uncertainties. The application of research in this area has been used widely for coordinate metrology and inspection of surface of physical objects. The results, which appear in [6], show that the computational uncertainty for measuring an Auto-body profile can be as high as 300 μm. Comparing this result with the effect of other sources of uncertainty in coordinate metrology such as equipment, environment, work-piece and operator [7], it can be seen that computational uncertainty in most cases can be even higher than the expanded uncertainty of all other sources. Under these conditions, the total expanded uncertainty of fitting computational algorithms can be unfeasible for the purpose of tolerance allocation.

The concept of integration of the three basic computation tasks, i.e. Point Measurement Planning (PMP), Substitute Geometry Estimation (SGE) and Deviation Zone Evaluation (DZE) is discussed in [8].

An integrated computational model can significantly solve the problem by providing an online share of information between the computational tasks. The architecture and general requirements for this integrated system in form of closed-loops between computational tasks are discussed in [8-9].

To benefit from potential advantages of integrated computational platform, sophisticated techniques for on-line generating the uncertainty information are required. Also, at each computational task, advanced methods are required to efficiently adapt the process based on the uncertainty information. To improve precision, an estimation of geometric deviations by DZE needs to be dynamically utilized by PMP to acquire the most useful data set from the measuring surface. Hence, gradual progress of DZE plays an important role in implementation of the integration concept. Moreover as the number of measured points increases, estimation of the optimum substitute geometry by SGE becomes a challenging task due to highly nonlinearity of the resulting optimization problem.

A loop between SGE and PMP is presented in [10]. Using a statistical pattern recognition technique the distribution of work-piece's geometric errors is studied and new sample points are captured accordingly. The results show that implementation of this method can reduce the uncertainty in inspection of a sculptured surface up to 60%.

DZE task in the traditional system is still in a preliminary stage and cannot provide a reliable knowledge about the pattern of work-piece's geometric deviations. It is required to develop methods that can predict the distribution of geometric deviations.

Evaluating the deviation zone based on the discrete measured points is generally a numerical evaluation based on a non-differential function. Thus, the problem of understanding the uncertainty of this evaluation is usually approached by researcher using numerical methods [11-14]. Two major sources of uncertainty in the computation tasks are the plug-in nature of the evaluation and the instability of the computational algorithm. These two issues arise respectively from the improper set of the measured data and the probability of trapping in the local minima in a highly non-linear optimization process. Numerous research projects are conducted to enhance the uncertainty inherent in each one of PMP and SGE tasks. However, the integration of these tasks with DZE and using the intermediate results to improve PMP and SGE tasks have not been studied properly in past literature.

The stability of the optimization problem in SGE is also has been under attention of researchers. It is shown in [11] that a closed-loop based operation of DZE and SGE can improve the convergence of the optimization by providing suitable initial conditions for partial fitting process. It is shown in [15] how alternative SGE objective functions can be defined based on the ultimate goal of the inspection process. The results show significant improvement in the fitting accuracy and stability.

Research on integration of mutual tasks has been also very limited. It has been attempted to develop a more suitable set of sampling points in an iterative fashion. An iterative sampling method is proposed in [16]. The method uses the available measured points and their normal vectors in an algorithm to interpolate the surface deviations between the measurement locations by a cubic polynomial to decide when and where additional sampling is required. Results show a significant reduction of uncertainty. However, this study doesn't provide any justification for its proposed interpolation algorithm.

The discrete points in the current work are generated by a FEA process, which are generated based on the utilized element's shape function. Selection of the most suitable group of these points is a complicated task that needs to be addressed in the future. For the purpose of the current research, the number and location of the measurements are selected exactly at the elements' nods.

3 METHODOLOGY

3.1 Allocation of Tolerance Zone

Considering having a predefined and fixed G_F, in order to maximize t in Equation 7, the zone specified by $(G_F \ominus G_I - K^{-1}F)$ needs to be maximized. We introduce a new geometric term, G^s, called substitute geometry which has exact geometric and topological properties of the original geometry an original, G, but it has been transferred to a different location and orientation using affine transformation maps.

$$G^s = T(\zeta) \times G \qquad \text{Eqn. 8}$$

where G^s is the substitute geometry of the original geometry G. Matrix $T(\zeta)$ is an orthogonal homogeneous transformation matrix which is a combination of three rotations about the three axes, following with three translations along the axes of the Cartesian coordinate system. Vector variables ζ consist of three rotation and three transformation parameters [15]. The substitute geometry has all the properties of the original geometry.

If one finds a specific substitute geometry of the final functioning geometry, G_F, that maximizes the expression in Equation 7, then the operator $\ominus$ can be also substituted by subtraction. labelling this optimum substitute geometry by G_F^{S*}, then Equation 7 can be rewritten as:

$$t = \alpha\,(G_F^{S*} - G_I - K^{-1}F) \qquad \text{Eqn. 9}$$

Therefore, the objective to find this optimum substitute geometry will be:

$$Objective\ Function = \underbrace{Max}_{\zeta}\,[Min\|G_F^S - (G_I + K^{-1}F)\|] \qquad \text{Eqn. 10}$$

where the statement inside the norm sign indicates the Euclidian distance of any point of $G_I + K^{-1}F$, from the temporary substitute geometry, G_F^S. If the optimization process successfully find the best set of Vector variables, ζ^*, then the optimum substitute for the final functioning geometry can be calculated using Equation 8.

If the tolerance zone is specified by uniform offsets from a nominal geometry, similar to the common practice and the way that it is defined in the variety of GD&T standards, then maximizing the minimum of Euclidian distance from G_F^S can be equivalent to minimizing the maximum distance of Euclidian distance from the substitute of the ideal initial geometry, G_I^S. Therefore the objective function in Equation 10 also can be achieved using:

$$Objective\ Function = \underbrace{Min}_{\zeta}\,[Max\|G_I^S - (G_I + K^{-1}F)\|] \qquad \text{Eqn. 11}$$

This is the L_∞-*norm* equation for minimum deviation zone fitting [15]. By utilizing a proper optimization process, the optimum vector variable ζ^* can be found in a way that the L_∞-*norm* equation is minimized. In this case the optimum substitute for the ideal initial geometry is calculated using the following Equation:

$$G_I^{S*} = T(\zeta^*) \times G_I \qquad \text{Eqn. 12}$$

The nearest point of the optimum substitute geometry, p_i^*, to the measured point, p_i, is called the corresponding point. The deviation of the measured points from the optimum substitute geometry, e_i, is the dot product of the vector from the corresponding point to the measured point, and the normal vector of the substitute geometry at the corresponding point, n_i^*.

$$e_i = \frac{(p_i^* - p_i) \cdot n_i^*}{|n_i^*|} \qquad p_i^* \in G_I^{S*} \qquad \text{Eqn. 13}$$

Evaluated geometric deviations, e_i, are labelled data captured from a continuous random variable, e with a probability density function, $f(e)$. This function is a result of all the geometric deformation of the ideal geometry due to applied loads.

3.2 The Best Substitute for Multi-Feature Geometries

Assume two actual geometric features, G_1' and G_2', are deformed geometric features due to combination of all loads and boundary conditions which are designed based on the specifications of two desired (ideal) geometric features, G_1 and G_2, respectively. Figure 1- a shows the two geometric features. The desired geometric relationship between the two geometric features is shown in Figure 1- b.

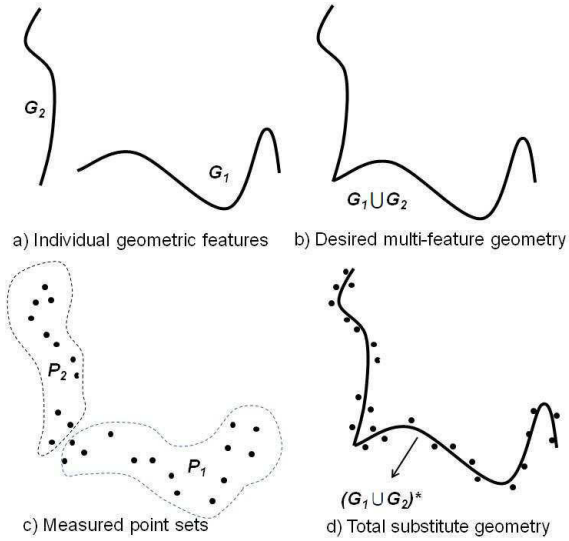

Fig. 1: Inspection of deformations in a multi- feature geometry.

Figure 1- c shows two sets of the measured points, P_{1_1} and P_2, which are assumed to be the sets of the best representative measured points from, G_1' and G_2', respectively. Let's use operator ∪ for the desired geometric relationship between two geometric features (Figure 1- b). Therefore the geometric tolerance between G_1 and G_2, is specified by the acceptable variations of $G_1 \cup G_2$ and the optimum substitute geometry is defined as:

$$G^* = (G_1 \cup G_2)^* \qquad \text{Eqn. 14}$$

4 IMPLEMENTATION

The beam- frame model is used for an implementation of the presented methodology. Finite Element Analysis determines nodal deflection of the design structure due to applied loading conditions using Equation 5. Once the deflections have been found, Equations 11 to 12 are used to allocate the

optimum tolerances for the structural components. As a case-study the three dimensional frame structure of a vehicle is analyzed (Figure 2).

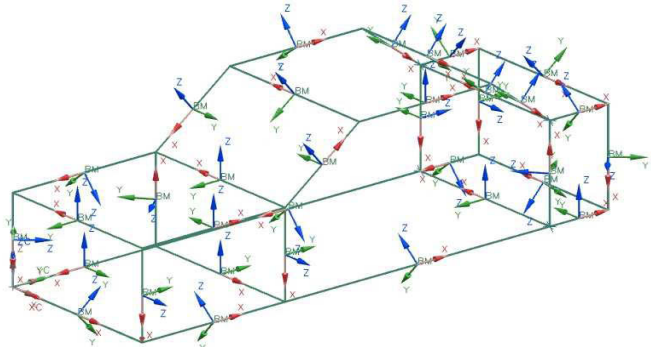

Fig. 2: Beam element model.

Figure 3-a shows 34 labeled beam elements exist in this structure. All of these elements have solid circular cross-sections. Figure 3-b shows the 20 nodes that connect these 34 beam elements. Table 1 presents elements information including their corresponding nodes and their radiuses and Table 2 presents the ideal coordinates of the 20 nodes.

Element #	Node 1	Node 2	Radius (mm)	Element #	Node 1	Node 2	Radius (mm)
1	1	2	60	18	9	10	60
2	1	3	60	19	10	12	60
3	1	5	60	20	11	12	60
4	2	4	60	21	11	13	60
5	2	6	60	22	12	14	60
6	3	4	60	23	13	15	60
7	3	7	60	24	13	19	60
8	4	8	60	25	13	14	60
9	5	6	60	26	14	16	60
10	5	7	60	27	14	20	60
11	5	15	60	27	15	16	60
12	6	8	60	29	15	17	60
13	6	16	60	30	16	18	60
14	7	8	60	31	17	18	60
15	7	9	60	32	17	19	60
16	8	10	60	33	18	20	60
17	9	11	60	34	19	20	60

Tab. 2: 34 labeled beam elements exist in the structure.

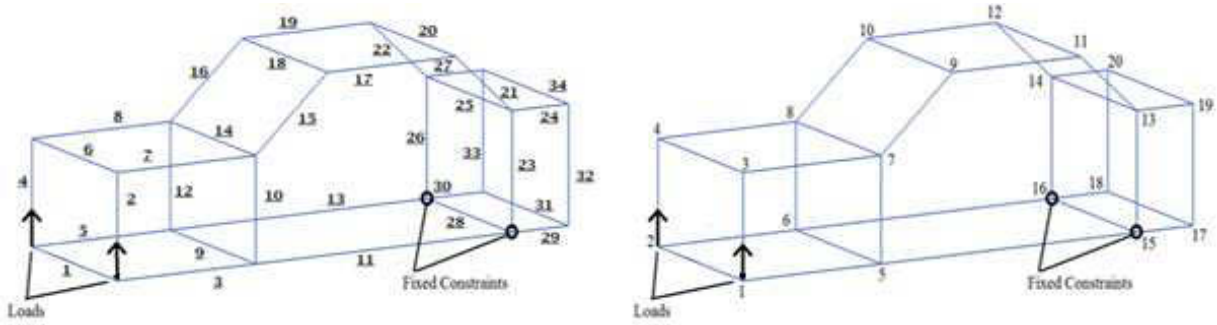

(a) (b)

Fig.3: Beam Element Geometry with Constraints and Loads: (a) elements' numbers (b) nodes' numbers.

Node #	X (m)	Y (m)	Z(m)	Node #	X (m)	Y (m)	Z(m)
1	0	0	0	11	3.3	0	1.35
2	0	1.5	0	12	3.3	1.5	1.35
3	0	0	0.8	13	3.85	0	0.9
4	0	1.5	0.8	14	3.85	1.5	0.9
5	1.35	0	0	15	3.85	0	0
6	1.35	1.5	0	16	3.85	1.5	0
7	1.35	0	0.8	17	4.4	0	0
8	1.35	1.5	0.8	18	4.4	1.5	0
9	2.05	0	1.35	19	4.4	0	0.9
10	3.05	1.5	1.35	20	4.4	1.5	0.9

Tab. 1: 20 labeled nodal ideal coordinates of the structure.

For this case study, without any loss of generality the bending deformation of the structure is analyzed. Figure 3 also shows the static loading and support condition of the structure causing a bending event. Vertical loads of 8696 N are applied at nodes 1 and 2 when a fixed boundary condition is applied at the rear of the structure (nodes 15 and 16). The amount of bending loads are calculated based on assumed weights for the vehicle components such as the drivetrain and passengers as well as the weight of the structure itself (Table 3).

Component	Weight (N)	Centre of Gravity Position (m)
Front Bumper	200	0
Powertrain	3000	0.65
Front Passengers & Seats	2000	2.2
Rear Passengers & Seats	2500	3
Fuel Tank	500	2.95
Luggage	950	4
Rear Bumper	300	4.4
Exhaust	350	2.5
Structure	7592	2.043

Tab. 3: Component weights for initial analysis.

After calculating the nodal deformation using Equations 5 and 6, and by assuming total of ±2mm for all elements as the total acceptable range of deviations, ΔG, the available tolerances for each element are calculated. The tolerance lower limit (Min. Tol.), upper limit (Max. Tol.), and total range for each element are listed in Table 4 as the original tolerances.

Element #	Min. Tol. Original (mm)	Max. Tol. Original (mm)	Tol. range Original (mm)	Min. Tol. Optimized (mm)	Max. Tol. Optimized (mm)	Tol. range Optimized (mm)	Increase of range of Tol.
1	- 0.82	0.82	1.64	- 5.40	5.68	11.08	574.25%
2	- 6.00	5.17	11.17	- 6.00	5.77	11.77	5.37%
3	- 0.82	2.60	3.42	- 5.30	5.43	10.73	213.78%
4	- 6.00	5.17	11.17	- 6.00	5.80	11.80	5.64%
5	- 0.82	2.60	3.42	- 5.57	5.70	11.27	229.57%
6	- 0.76	0.76	1.51	- 5.43	5.72	11.15	637.22%
7	- 0.82	2.60	3.42	- 5.32	6.00	11.32	231.02%
8	- 6.00	0.82	6.82	- 5.60	6.00	11.60	70.03%
9	- 2.60	2.60	5.19	- 5.29	5.57	10.86	108.97%
10	- 6.00	5.17	11.17	- 6.00	5.75	11.75	5.15%
11	- 2.60	6.00	8.60	- 4.96	5.30	10.26	19.38%
12	- 6.00	5.17	11.17	- 6.00	5.78	11.78	5.41%
13	- 2.60	6.00	8.60	- 5.23	5.57	10.81	25.70%
14	- 2.50	2.50	4.99	- 5.32	5.60	10.92	118.57%
15	- 3.84	6.00	9.84	- 6.00	5.43	11.43	16.18%
16	- 6.00	3.02	9.02	- 6.00	4.97	10.97	21.62%
17	- 5.17	3.25	8.41	- 5.52	5.14	10.66	26.76%
18	- 3.03	3.03	6.06	- 4.96	5.53	10.49	72.98%
19	- 6.00	3.25	9.25	- 4.96	5.42	10.38	12.30%
20	- 4.43	4.43	8.86	- 5.41	5.14	10.54	19.05%
21	- 5.58	4.51	10.09	- 5.07	6.00	11.07	9.62%
22	- 6.00	4.51	10.51	- 5.26	6.00	11.26	7.12%
23	- 6.00	5.35	11.35	- 5.76	5.70	11.46	0.94%
24	- 5.68	5.99	11.67	- 5.33	4.99	10.32	- 11.57%
25	- 5.35	5.35	10.70	- 5.22	4.96	10.18	- 4.83%
26	- 6.00	5.35	11.35	- 5.72	5.72	11.44	0.83%
27	- 6.00	5.68	11.68	- 5.61	5.27	10.88	- 6.82%
27	- 6.00	6.00	12.00	- 4.96	5.24	10.20	- 14.96%
29	- 5.68	6.00	11.68	- 5.30	4.96	10.26	- 12.14%
30	- 6.00	5.68	11.68	- 5.56	5.23	10.79	- 7.60%
31	- 5.68	5.68	11.36	- 5.31	5.58	10.89	- 4.19%
32	- 6.00	5.35	11.35	- 5.75	5.69	11.44	0.82%
33	- 6.00	5.35	11.35	- 5.72	5.71	11.43	0.71%
34	- 5.27	5.27	10.55	- 5.53	5.29	10.82	2.60%

Tab. 4: Allocate tolerances for 34 labeled beam elements after and before optimization.

Using the optimization process presented by Equations 11 the optimum vector of the transformation variables, ζ^*, is calculated as follows:

Rotation about X- axis	Rotation about Y- axis	Rotation about Z- axis	Translation along X- axis	Translation along Y- axis	Translation along Z- axis
- 0.0002 rad	- 0.0012 rad	- 0.00002 rad	- 0.0210 mm	- 0.0117 mm	5.7101 mm

Tab. 5: Optimum vector of the transformation variables.

By employing this optimum transformation vector the optimized allocated tolerances are calculated. Table 4 presents lower limit (Min. Tol.), upper limit (Max. Tol.), and the total range of optimized tolerance for each element. The last column of Table 4 lists the percentage of increase of tolerance range for each element after optimization comparing to the original tolerances. It can be seen that in average the total tolerance range of element is increased for 69.98%.

Figures 4- a and 4- b demonstrate distribution of the tolerance upper and lower limits for elements before and after optimization, respectively. Comparing the two figures shows that the allocated tolerance zones for the elements are maximized after applying the presented optimization process.

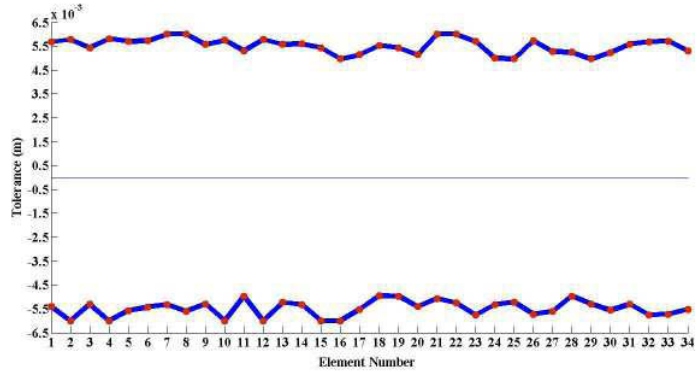

(b)

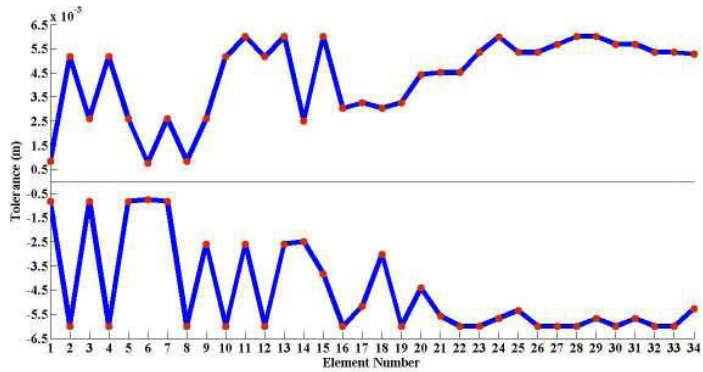

(a)

Fig. 4: Distribution of the tolerance upper and lower limits for elements (a) original allocated tolerances (b) tolerances after proposed optimization processes.

5 CONCLUSION

A new approach to allocate proper design tolerances considering the actual deformations of the mechanical parts and components due to their loading condition is presented. Methodology and a practical procedure are detailed and it is shown that implementation of the developed methodology allocates maximized tolerance zones for the components without losing the desired accuracy and functionality of the final product.

Allocating unnecessary tight tolerances to design usually increases manufacturing cost and time. Utilizing the concept and methodology presented in this paper eliminates this waste. The presented case-study demonstrates that by employing the proposed procedure for a typical structural design under a typical loading condition, the increase of tolerance zone can be as significant as 69%.

ACKNOWLEDGMENT

The research support provided by the Natural Science and Engineering Research Council of Canada (NSERC) is greatly appreciated.

REFERENCES

[1] Li, Bing; Yang, Xiaojun; Hu, Ying; Zhang, Donglai: Quality design of tolerance allocation for sheet metal assembly with resistance spot weld, International Journal of Production Research, 47, 2009, 1695–1711 http://dx.doi.org/10.1080/00207540701644193

[2] Barari, A.; ElMaraghy H. A.; ElMaraghy W. A.: Design For Machining of Sculptured Surfaces - A Computational platform, ASME Transaction- Journal of Computing and Information Science in Engineering, 9, 2009

[3] Barari, A.; ElMaraghy, H. A.; Orban, P.: NURBS Representation of Actual Machined Surfaces, International Journal of Computer Integrated Manufacturing, 22, 2009, 395 – 410 http://dx.doi.org/10.1080/09511920802392730

[4] Logan, Daryl L.: A First Course in the Finite Element Method, Thomsen Canada Limited, Toronto, Canada, 2007

[5] Juster, Neal P.; Manarvi, Anjum Irfan: Framework of an integrated tolerance synthesis model and using FE simulation as a virtual tool for tolerance allocation in assembly design, Journal of Materials Processing Technology, 2004, 182–193

[6] Barari, A.: Sources of Uncertainty in Coordinate Metrology of Automotive Body, CD Proc. of 2nd CIRP International Conference on Assembly Tech. and Systems, 2008 Toronto

[7] Barari, A.: Automotive- Body Inspection Uncertainty Due to Computational Complexity, International Journal of Vehicle Design, 57, 2011

[8] Barari, A.; Pop-Iliev, R.: Closed-Loop Engineering in Adaptable Design and Manufacturing, CIRP International Conference on Changeable, Agile, Reconfigurable and Virtual Production, 2007

[9] Barari, A.; Pop-Iliev R.: Reducing Rigidity by Implementing Closed-Loop Engineering in Adaptable Design and Manufacturing Systems, Journal of Manufacturing Systems, 2009, 47-54, DOI information: 10.1016/j.jmsy.2009.04.003.

[10] Barari, A.; ElMaraghy H. A.; Knopf, G. K.: Guided sampling to reduce uncertainty of minimum zone estimation, ASME Transaction- Journal of Computing and Information Science in Engineering, 7, 2007, 360-371 http://dx.doi.org/10.1115/1.2798114

[11] Choi, W.; Kurfess, T. R.; Cagan, J.: Sampling Uncertainty in Coordinate Measurement Data Analysis, Precision Engineering, 22, 1998, 153-163 http://dx.doi.org/10.1016/S0141-6359(98)00011-7

[12] Sprauel, J. M.; Linares, J. M.; Bachmann, J.; Bourdet, P.: Uncertainties in CMM Measurements, Control of ISO Specifications, Annals of CIRP- Manufacturing Technology, 52, 2003, 423-426.

[13] Choi, W.; Kurfess, T. R.: Uncertainty of Extreme Fit Evaluation for Three-Dimensional Measurement Data Analysis, Computer-Aided Design, 30, 1998, 549-557 http://dx.doi.org/10.1016/S0010-4485(98)00012-8

[14] Yau, H. T.: A Model-Based Approach to Form Tolerance Evaluation Using Non-Uniform Rational B-Splines, Robotics and Computer Integrated Manufacturing, 15, 1999, 283-295 http://dx.doi.org/10.1016/S0736-5845(99)00012-5

[15] ElMaraghy, H. A.; Barari, A.; Knopf, G. K.: Integrated inspection and machining for maximum conformance to design tolerances, Annals of CIRP-Manufacturing Technology, 53/1, 2004, 411-416 http://dx.doi.org/10.1016/S0007-8506(07)60728-8

[16] Edgeworth, R.; Wilhelm, R. G.: Adaptive Sampling for Coordinate Metrology, Precision Engineering, 23, 1999, 144-154 http://dx.doi.org/10.1016/S0141-6359(99)00004-5